Directional solidification under stress

Isabelle Cantat,[1] Klaus Kassner,[2] Chaouqi Misbah,[1] and Heiner Müller-Krumbhaar[3]
[1]*Laboratoire de Spectrométrie Physique, Université Joseph Fourier (CNRS), Grenoble I, Boîte Postale 87, Saint-Martin d'Hères, 38402 Cedex, France*
[2]*Institut für Theoretische Physik Otto-von-Guericke-Universität, Magdeburg Postfach 4120, D-39016 Magdeburg, Germany*
[3]*Institut für Festkörperforschung des Forschungszentrums Jülich, 52425 Jülich, Germany*
(Received 31 March 1998)

Directional solidification under uniaxial stress is analyzed. In the absence of stress, it is well known that the moving planar front undergoes a morphological Mullins-Sekerka (MS) instability. Under uniaxial stress, even an interface at rest develops an instability known by the names of Asaro, Tiller, and Grinfeld (ATG). This paper analyzes the coupling between these two instabilities, a situation on which we have recently given a brief account [Durand *et al.*, Phys. Rev. Lett. **76**, 3013 (1996)]. We discover that under favorable circumstances a weak uniaxial stress of the order of 1 bar leads to a dramatic change of the Mullins-Sekerka instability. The threshold, together with the microstructure scale, are shifted by amounts going up to one (or several) decade(s). This effect should open new lines of both experimental and theoretical inquiries. A weakly nonlinear analysis is presented by means of a Landau expansion. It is known that the MS bifurcation is subcritical for a small enough solute partition coefficient, and is supercritical otherwise. The ATG instability is always subcritical. The nonlinear evolution of the ATG instability leads to cusps which grow unstably, leading ultimately to the fracture threshold. It is shown here that due to a subtle coupling between both instabilities, the MS bifurcation in its supercritical regime may cause the MS-ATG coupled bifurcation to be supercritical. Discussions and outlooks are presented. In particular it is appealing to speculate that the creation of giant causeways in igneous rocks can be interpreted within the present context. [S1063-651X(98)07010-X]

PACS number(s): 81.10.Aj, 05.70.Fh, 81.30.Fb, 68.70.+w

I. INTRODUCTION

It is by now well documented that a moving solidification front in an external thermal gradient (directional solidification) undergoes a morphological Mullins-Sekerka (MS) instability [1] above a critical growth velocity. The initially planar interface bifurcates into a cellular structure, which itself bifurcates to deep cells and then to dendrites at higher speed [2]. The cellular structure may also, at both small [3] and large speeds [4], experience symmetry-breaking instabilities, leading ultimately to spatiotemporal chaos. The scale of the patterns is roughly determined by $\lambda_{\mathrm{MS}} \sim \sqrt{l d_0}$, which is a compromise between two competing scales: the destabilizing diffusion length $l \sim D/V$ (where V is the pulling speed and D the solute diffusion constant) and the chemical capillary length $d_0 = \gamma T_M / L \Delta T$ (L is the latent heat per unit volume, γ the surface tension, T_M the melting temperature, and ΔT the freezing range). λ lies roughly in the 10–100-μm range. More recently, Grinfeld [5] brought out the idea, which was earlier presented by Asaro and Tiller [6], that when a solid is subject to a uniaxial stress (i.e., when $\sigma_0 \equiv \sigma_{xx} - \sigma_{zz} \neq 0$, σ_{ij} is the stress tensor) the solid-liquid (or solid-vacuum) planar interface becomes unstable and turns onto a cellular structure [Asaro-Tiller-Grinfield (ATG) instability]. This instability is of elastic origin: a surface corrugation reduces the stored elastic energy. It must be emphasized that this corrugation does not correspond to a bending of the solid (as it is the case when one applies a longitudinal pressure to a thin rod). Here, in contrast, the instability materializes itself via mass transport and is independent of whether the stresses are tensile or compressive. When the solid is in contact with vacuum (a situation encountered in heteroepitaxy, for example, where the lattice mismatch is the source of axial stresses), the instability takes place via mass surface diffusion in most cases but might also be supported by other transport processes (vacancy diffusion, impurity diffusion, etc.). Though the instability is potentially present in any strained solid, mass transport is needed to build up the fluctuation. The time scale which is needed depends strongly on temperature. We shall review these points in this paper. The scale of the pattern is approximately given by $\lambda_{\mathrm{ATG}} \sim \gamma E / \sigma_0^2$ (E is the Young modulus). This leads to a scale in the range of 10–100 nm for typical heteroepitaxy. When the solid is in contact with its melt, however, the liquid provides a mass reservoir, and the ATG instability manifests itself by a melting-crystallization process. That is to say chemical attachment or detachment at the front becomes the limiting factor for the development of the instability.

When the solid is in the bottom and the liquid on top, any corrugation raises the level of the solid and lowers that of the liquid in an alternating manner. If the corrugation wavelength is not too small (see below for more detail), then gravity can lay a stabilizing role. The typical length scale is expected to be of the order of the gravitational capillary length (as is the case for gravity waves) $\lambda_{\mathrm{ATG}} \sim \sqrt{\gamma / g \Delta \rho}$ (g is the gravity, and $\Delta \rho$ the solid-liquid densities difference). This leads to a scale in the range 0.1–1 cm. It must be noted that the wavelength given above could as well be expressed in terms of a stress. Indeed, the above value corresponds to the threshold one, where the gravity effect (which is stabilizing) precisely counterbalance the destabilizing effect due to stress. An impressive experiment was performed by Balibar and co-workers [7] on solid He^4 in contact with the superfluid, and has unambiguously demon-

strated the ATG instability taking place on a scale of 0.7 cm. Nonlinear calculations have shown that such an instability may lead to fracture, though the external stress is a small fraction of the atmospheric pressure [8].

These front instabilities are important focuses of research both on the technological and fundamental levels, and they seem to embrace disparate situations ranging from low-dimensional nanostructures [9] (e.g., quantum dots), to geology [10]. However, from the above scale estimates one would naively expect that there is (virtually) no coupling between the MS and ATG instabilities given the disparate lengths on which they operate. We show here that in contrast there is clearly strong interaction in the case of directional solidification. Indeed the external thermal gradient G, combined with other parameters, will be shown to play the role of an effective gravity $g_{\rm eff}\Delta\rho = LG/T_M$, where for typical materials we find that $g_{\rm eff} = (10^3 - 10^4)g$ (i.e., the effective gravity is several orders of magnitude larger than the real gravity). This brings down the scale of the ATG instability to the range 10–100 μm, which is in the same range as the MS scale, and strong coupling between the two instabilities must be expected. An important result which follows from our analysis is that the MS stability tongue exhibits a dramatic change in the presence of weak uniaxial stress, of the order of the atmospheric pressure. In particular, the velocity threshold is reduced by a factor of about 10, and the microstructure scale is decreased at low speed and increased at large speed by the same amount. Such an effect is clearly not devoid of experimental testability. Usually, producing small scales microstructures necessitates solidification at higher speeds which are only accessible by means of laser melting or resolidification. Furthermore, it is very difficult to have precise quantitative results. For example, accurate estimates of the thermal gradient are difficult to obtain. It appears that solidification under stress can lead, even at moderate velocities, to small scales. We shall discuss this point in detail in this paper.

For pure directional solidification, the planar liquid-solid interface undergoes a subcritical bifurcation in the standard velocity range (ranging from 1 to 100 μm/s) if the solute partition coefficient is small enough (smaller than approximately 0.45 [11]), and a supercritical biforcation otherwise. Nozières [12] showed that the ATG instability is always subcritical. A fully nonlinear analysis shows [8] that the ATG instability develops and deep grooves grow unstably, leading ultimately to fracture generation. Here a subtle interplay between the two instabilities in the nonlinear regime is found. Depending on the parameters, the bifurcation can either always be subcritical regardless of the value of the partition coefficient, or can become supercritical if the partition coefficient is not too small, though the ATG instability is always subcritical. Thus a stressed solid, which would develop grooves growing unstably without bound, can develop a smooth and gentle front when driven away from equilibrium.

The scheme of this paper is as follows. Section II will give a short review, plus some new results on the pure ATG instability. In Sec. III we write down the model equations of the system including directional solidification. Section IV presents the linearized version of the coupled instabilities, and the far-reaching consequences. Section V is devoted to the weakly nonlinear analysis, to the determination of the nature of the bifurcation. A summary and an outlook are the subjects of Sec. VI. Technical details and useful derivations are given in the appendixes.

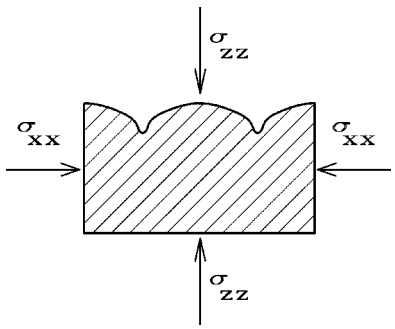

FIG. 1. The configuration of surface forces after application of a small perturbation to a prestrained solid.

II. ATG INSTABILITY

A. General formulation

Since the ATG instability has been identified rather recently, we feel it worthwhile to discuss it separately, and to present some of its potential applications in other fields. We shall then present its coupling to the MS instability in Sec. III.

We wish to describe the behavior of a solid submitted to uniaxial stress and in contact with its melt. Let the two-phase system initially be in equilibrium in a gravitational field (which is ordinary gravity for the pure ATG instability, but will be replaced with effective gravity in the case of directional solidification).

The applied external stress is assumed to act along the x direction. Our choice of a coordinate system can be inferred from Fig. 1. We shall see in this subsection that an instability arises and may lead to a corrugation of the solid-liquid interface via a melting-crystallization phenomenon.

For simplicity, we restrict ourselves to planar strain and isotropic elastic properties of the solid, i.e., we set the strain component $u_{yy} = 0$, which implies, via Hooke's law,

$$\sigma_{ij} = \frac{E}{1+\sigma}\left(u_{ij} + \frac{\sigma}{1-2\sigma} u_{kk}\delta_{ij} \right), \tag{1}$$

where σ_{ij} is the stress tensor (repeated subscripts are to be summed over), and σ the Poisson ratio.

A simple intuitive argument exhibiting the origin of the instability was given by Nozières [13]. Suppose there is a small fluctuation of the interface at constant strain. Then the mechanical equilibrium conditions at the interface are no longer satisfied. The forces on the interface, exerted by the liquid, due to its pressure p_l, and by the solid, due to the anisotropic stress tensor, no, longer compensate for one another. In particular, there is a net *tangential* force. (To linear order in the perturbation, the normal forces *do* compensate for one another.) Mechanical equilibrium is broken, and the solid will relax under the tangential force. The relaxation cannot lead back to the original state (it changes the strain), so there is an instability.

In the following we will assume that the system is above the temperature of its roughening transition, i.e., the attach-

ment kinetics are fast, resulting in a growth velocity (normal to the interface) that is proportional to the difference in chemical potential between the liquid and the solid:

$$v_n = -k_v(\mu_s - \mu_l) \equiv -k_v \Delta\mu. \tag{2}$$

Since the proportionality constant k_v is large, the system will be in a state with small $\Delta\mu$, i.e., close to local equilibrium, whenever the growth velocity is limited by material diffusion, as is the case in the solidification of alloys. Therefore, in treating directional solidification, we will not use Eq. (2) directly, but rather exploit the mass conservation law to be presented in Sec. III. The present formulation would be valid for the experiment on helium [7], where the prevailing dissipation mechanism is attachment/detachment at the front.

However, Eq. (2) will serve to determine the concentration field at the interface in an extension of the Gibbs-Thomson condition to the elastic case. In the appendixes, we show that $\Delta\mu$ is given, to leading order, by

$$\Delta\mu = \frac{1-\sigma^2}{2E}(\sigma_{tt} - \sigma_{nn})^2 + \gamma\tilde{\kappa} + \Delta\rho g \tilde{\zeta}(x). \tag{3}$$

Herein $\sigma_{tt} = t_i \sigma_{ij} t_j$ and $\sigma_{nn} = n_i \sigma_{ij} n_j$ (n_i and t_i are the ith components of the normal and the tangent unit vectors, respectively) are the purely tangential and normal components of the stress tensor, respectively, γ is the surface tension, $\tilde{\kappa}$ is the interface curvature (in dimensional form), $\Delta\rho = \rho_s - \rho_l$ is the difference of the solid and liquid densities, $\tilde{\zeta}(x)$ is the position of the solid-liquid interface, and g is the gravitational constant. For convenience, we refer chemical potentials to the unit volume of a piece of solid. This definition differs from the conventional one, referring to the unit mass, by a constant factor ρ_s. Using our convention, we can omit this factor in the denominators of Eq. (3) and in other formulas.

First, the elastic field must be computed. For the one-dimensional deformations considered here, it is convenient to make use of the Airy function $\chi(x,z)$, which is related to the stress tensor via

$$\sigma_{xx} = \frac{\partial^2 \chi}{\partial z^2}, \tag{4}$$

$$\sigma_{zz} = \frac{\partial^2 \chi}{\partial x^2}, \tag{5}$$

$$\sigma_{xz} = -\frac{\partial^2 \chi}{\partial x \partial z}. \tag{6}$$

It can be shown [14] from the Lamé equations that χ obeys the biharmonic equation

$$\nabla^2 \nabla^2 \chi = 0. \tag{7}$$

The elastic problem must be supplemented with mechanical equilibrium conditions at the front. These are

$$\sigma_{nn} = -p_l, \quad \sigma_{nt} = 0, \tag{8}$$

where p_l is the hydrostatic liquid pressure, and $\sigma_{nn} = n_i \sigma_{ij} n_j$, $\sigma_{nt} = n_i \sigma_{ij} t_j$. Before proceeding further, some remarks are in order. (i) We have neglected capillary effects in the above mechanical equilibrium condition ($\sigma_{nn} = -p_l$). It can be shown [15] that this is legitimate up to corrections of the order of σ_0/E, which is large only close to the fracture threshold. (ii) We consider the static version of elasticity, which is obviously legitimate for small velocities as compared to the sound speed. (iii) An important point which must be emphasized concerns the elastic effect due to the incorporation of the solute in the solid. This should basically alter the equilibrium condition which relates the concentrations on both phases. As shown by Spencer *et al.* [16], this leads to small effects on the stability.

The boundary conditions (8) read, explicitly,

$$p_l + n_x^2 \sigma_{xx} + 2\sigma_{xz} n_x n_z + n_z^2 \sigma_{zz} = 0, \tag{9}$$

$$n_x t_x \sigma_{xx} + n_x t_z \sigma_{xz} + n_z t_x \sigma_{xz} + n_z t_z \sigma_{zz} = 0. \tag{10}$$

The normal and the tangent are related to the interface position $z = \tilde{\zeta}(x,t)$ by

$$(n_x, n_z) = (-\partial\tilde{\zeta}/\partial x, 1)/\sqrt{1 + (\partial\tilde{\zeta}/\partial x)^2}, \tag{11}$$

$$(t_x, t_z) = (1, \partial\tilde{\zeta}/\partial x)/\sqrt{1 + (\partial\tilde{\zeta}/\partial x)^2}. \tag{12}$$

Let $\sigma_{ij}^{(0)}$ denote the strain contribution of the prestrained situation corresponding to the planar front solution. When the solid surface deforms, the strain configuration will change. For a general interface morphology the problem can be tackled only numerically. Throughout this paper we will be concerned with linear and weakly nonlinear front excursions where analytical solutions can be obtained. Let ϵ (a small quantity) denote the strength of the surface modulation [$\zeta(x,t) = \epsilon h(x,t)$, where h is of order 1]. The strain can be written as

$$\sigma_{ij} = \sigma_{ij}^{(0)} + \epsilon\sigma_{ij}^{(1)} + \epsilon^2\sigma_{ij}^{(2)} + \epsilon^3\sigma_{ij}^{(3)} + \cdots. \tag{13}$$

We shall later see that one needs to go up to third order in ϵ. The boundary conditions (9) and (10) become, to that order,

$$\begin{aligned} 0 = {} & p_l + \sigma_{zz}^{(0)} + \epsilon\sigma_{zz}^{(1)} + \epsilon^2[h'^2\sigma_0 - 2h'\sigma_{xz}^{(1)} + \sigma_{zz}^{(2)}] \\ & + \epsilon^3[(\sigma_{xx}^{(1)} - \sigma_{zz}^{(1)})h'^2 - 2h'\sigma_{xz}^{(2)}] + \cdots, \end{aligned} \tag{14}$$

$$\begin{aligned} 0 = {} & \epsilon[-\sigma_0 h' + \sigma_{xz}^{(1)}] + \epsilon^2[\sigma_{xz}^{(2)} - h'(\sigma_{xx}^{(1)} - \sigma_{zz}^{(1)})] \\ & + \epsilon^3[h'(\sigma_{zz}^{(2)} - \sigma_{xx}^{(2)}) + \sigma_0 h'^3 + \sigma_{xz}^{(3)} - 2h'^2\sigma_{xz}^{(1)}\sigma_{zz}^{(3)}] \\ & + \cdots. \end{aligned} \tag{15}$$

We shall need σ_{tt} as well [see Eq. (3)], which takes the form

$$\begin{aligned} \sigma_{tt} = {} & \sigma_{xx}^{(0)} + \epsilon\sigma_{xx}^{(1)} + \epsilon^2[-h'^2\sigma_0 + 2h'\sigma_{xz}^{(1)} + \sigma_{xx}^{(2)}] \\ & + \epsilon^3[(\sigma_{zz}^{(1)} - \sigma_{xx}^{(1)})h'^2 + 2h'\sigma_{xz}^{(2)} + \sigma_{xx}^{(3)}] + \cdots. \end{aligned} \tag{16}$$

These quantities are understood to be evaluated at the front $z = \epsilon h(x,t)$. The quantity $h(x,t)$ will also be expanded in power series of ϵ

$$h(x,t)=h_0(x,t)+\epsilon h_1(x,t)+\cdots. \tag{17}$$

Similarly we decompose the Airy function as

$$\chi(x,z,t)=\chi_0(x,z)+\epsilon\chi_1(x,z,t)+\cdots, \tag{18}$$

where we have introduced the notation $\sigma_0\equiv\sigma_{xx}^{(0)}-\sigma_{zz}^{(0)}$. Because $\sigma_0\neq 0$, we usually say that the system is subject to a uniaxial stress. As it will appear soon, this uniaxial stress directly induces a morphological instability of the planar surface.

In a planar geometry $\epsilon\equiv 0$. Thus the first boundary condition from Eqs. (14) and (15) takes the form $\sigma_{zz}^{(0)}=-p_l$ (and the second one is automatically satisfied). Moreover, we must have $\sigma_{xz}^{(0)}=0$, since no shear is imposed. It is clear that the Airy function must, though the surface is planar, depend on x and z in order to fulfill the boundary conditions. It is a simple matter to check that

$$\chi_0(x,z)=-p_l\frac{x^2}{2}+(\sigma_0-p_l)\frac{z^2}{2} \tag{19}$$

solves Eq. (7) together with boundary conditions, and provides $\sigma_{xz}^{(0)}=0$.

B. Linear analysis: The ATG instability

The planar solution (19), together with $\zeta=\epsilon h_0=0$, is unstable against corrugations as long as $\sigma_0\neq 0$. This is what we will show now. Suppose that the interface undergoes a fluctuation $h_1(x,t)=h_{11}e^{iqx+\omega t}$, where h_{11} is a constant amplitude. Because in the linear regime the Fourier modes are independent, we consider one Fourier component only. To calculate the elastic field we insert χ [Eq. (18)] into Eq. (7). We easily obtain that $\chi_1=(a+bz)e^{iqx+qz+\omega t}$, where a and b are integration constants (the condition $\chi=0$ when $z\to-\infty$ is used). These are easily determined from Eqs. (14) and (15) to order ϵ after expressing σ_{ij} in terms of χ. We straightforwardly obtain $a=0$ and $b=-\sigma_0 h_{11}$ (h_{11} is yet an undetermined constant). In order to determine the stability condition, one has to evaluate the chemical potential (3) induced by a shape fluctuation. For that purpose one needs to evaluate the stress contribution [Eq. (16)]

$$\sigma_{tt}-\sigma_{nn}=\sigma_0[1-2q\epsilon h_1(x,t)]. \tag{20}$$

so that the difference in chemical potential (3) becomes

$$\Delta\mu=\frac{(1-\sigma^2)\sigma_0^2}{2E}[1-4q\epsilon h_1]+\epsilon\gamma q^2 h_1+g\Delta\rho(\epsilon h_1+h_{00}) \tag{21}$$

The first term is composed of the zeroth-order contribution and the first-order one. The zeroth-order contribution is positive, meaning that a stress increases the solid chemical potential and renders it unfavorable. A melting of the planar front thus occurs. This melting is to be counterbalanced by the gravity effect. This is why we have added, in the gravity term, the constant contribution h_{00} (the origin was up to now arbitrary). The new position of the solid-liquid interface is now $h_{00}=-(1-\sigma^2)\sigma_0^2/(2g\Delta\rho E)$ if the unstrained interface is at $z=0$. Thus from now on we shall redefine the origin at the new position.

To order ϵ, $\Delta\mu$ is lowered when h_1 [$h_1\simeq\cos(qx)$] is positive, and increased otherwise. That is to say the solid chemical potential is lowered close to the maximum and increased close to the minimum. Thus if a protuberance takes place the crystallization will be favored on top (i.e., in the convex part of the interface), and melting occurs in the bottom (in the concave part). This is the ATG instability. It must be emphasized that this is a chemical instability and not a mechanical one: the instability materializes itself through a melting or growth process, and not as a buckling of the solid. If the solid were in contact with vacuum, then the instability would be expressed via mass transport along the surface (surface diffusion). The presence of q in front of h_1 in Eq. (21) reflects the fact that the stress relaxation penetrates over a distance of order $1/q$ into the bulk.

Using the fact that $v_n\simeq\partial h_1/\partial t=\omega h_1$ in the linear regime, and making use of Eq. (2) we obtain, using Eq. (21), the dispersion relation

$$\omega=k_v\left[\frac{2\sigma_0^2(1-\sigma^2)}{E}q-\gamma q^2-\Delta\rho g\right]. \tag{22}$$

Here one clearly sees the destabilizing effect of elasticity, and the stabilizing effects due both to surface tension and gravity.

In the absence of gravity the planar surface is unstable however small the uniaxial stress σ_0 is against perturbations of wave numbers smaller than

$$q_c=\frac{2(1-\sigma^2)\sigma_0^2}{E\gamma}. \tag{23}$$

If one uses a small fraction of an atmospheric pressure (as used for helium) for the uniaxial stress (about 10^4 cgs; 0.01 bar), $E\sim 10^9$ and $\gamma\sim 0.1$ cgs, we obtain $\lambda_c\sim 10$ cm.

In the presence of gravity there is a critical stress above which the surface becomes unstable. This stress provides a critical wave number for the instability. These threshold values are obtained by solving $\omega=\partial\omega/\partial q=0$. This yields

$$\sigma_{0c}^2=\frac{E}{1-\sigma^2}\sqrt{\gamma g\Delta\rho},\quad q_c=\sqrt{\frac{g\Delta\rho}{\gamma}}. \tag{24}$$

The threshold wavelength $2\pi/q_c$ is nothing but the gravity capillary length, which is in general of the order a few mm. This is consistent with the measurement of Ref. [7]. The corresponding threshold stress for ^{4}He is of about $\sigma_{0c}\sim 10^4$ cgs.

Since the ATG instability may have implications on other systems, it is appropriate to make a short digression. In heteroepitaxy a thin film is grown on a substrate. The lattice mismatch causes a film to develop a strain. Provided that no misfit dislocations occur, the stress in the film relaxes via an elastic deformation. We can recalculate the chemical potential for a strained film. If the thickness is small, one has to take into account the finite depth effect (precisely as with shallow water waves). The chemical potential is approxi-

mately (only the linear part is considered) given by (where the substrate is supposed to be rigid)

$$\Delta\mu=\left[2\frac{(1-\sigma^2)\sigma_0^2}{E}q^2d-\gamma q^2\right]h_1, \tag{25}$$

where d is the film thickness. One thus sees that relaxation takes place after a critical thickness of order

$$d_c\sim\frac{\gamma E}{\sigma_0^2}, \tag{26}$$

where we have neglected σ^2 in comparison to 1 (for most situations $\sigma\sim 1/3$). The uniaxial stress $\sigma_0\sim E(\Delta a/a)$ ($\Delta a/a$ is the lattice mismatch). On the other hand, generally $\gamma/E\sim a$ (because there is within a material no other intrinsic length scale than the atomic one), so that $d_c\sim a/(\Delta a/a)^2$. A large enough mismatch is $(\Delta a/a)\sim 1\%$, so that $d_c\sim 10^4 a$. There are many situations in molecular beam epitaxy where the critical thickness for the transition from layer by layer growth into a three-dimensional (3D) growth occurs only after a few monolayers. A typical example is the case of Ge/Si, free of dislocations, where the transition into 3D growth (the so-called Stranski-Krastanow [17] mode) takes place only after 2–3 ML [18]. This dilemma has not been resolved to date [20]. It is important to note that elastic effects seem to play an important role in the fabrication of quantum dots. This topic is of much current interest, and where island self-organization with a size of about 100 nm appears spontaneously [19], it is most likely due to (probably not solely) an instability of the present type.

Finally, it is important to note that although an elastic instability is potentially present, its manifestation time is finite. It is fixed by the slowest dissipation mechanism. For ^{4}He, kinetic attchment seems to be the limiting factor. The order of magnitude of k_v (the kinetic coefficient entering 2) is of about $\rho k_v\sim 0.01$ cgs [7] [$1/(\rho k_v)$ has a dimension of a velocity; its value is about 100 cm/s] provides for the fastest growing mode a typical time of the order of 1–10 s. This is quite consistent with experiments. For the case of an impure liquid (Sec. III) mass diffusion in the liquid phase limits the instability. Finally, when a solid is in contact with vacuum, mass transport along the surface is the prevailing dissipation mechanism. The time scale was discussed in Ref. [20], and it depends on the surface diffusion constant which is a thermally activated quantity. It is shown there that time scale is of the order of $0.1–1/D$ cgs, where D is diffusion constant. One needs at least diffusion constants of the order of 10^{-1}–10^{-3} cm^2/s to observe the instability within a few seconds to a few minutes. Usually one expects diffusion constant to be much smaller, implying a large time for the instability development. This problem is currently being explored.

III. MODEL EQUATIONS

Let us now treat the coupling between the MS and ATG instabilities. In Ref. [21], we considered only the one-sided model, appropriate for most solids, in order to keep the presentation concise. Here we give the general case, which is only slightly more involved. In the liquid phase, the reduced concentration field $u=(c-c_\infty)/\Delta c$ (Δc is the miscibility gap and c_∞ is the concentration far ahead of the front) obeys the diffusion equation written in the laboratory frame

$$\Delta u+2\frac{\partial u}{\partial z}=\frac{\partial u}{\partial t}, \tag{27}$$

where lengths and time are reduced by $l=2D/V$ and $\tau=l^2/D$, respectively, D being the mass diffusion constant, and V the speed at which the sample is pulled through the thermal gradient field. A similar equation holds for the solid with a prefactor $\nu=D_s/D$, where D_s is the diffusivity in the solid, in front of the Laplacian. At the interface, u is subject to the mass conservation condition

$$v_n[u-k(u-1)]=-\left.\frac{\partial u}{\partial n}\right|_l+\nu\left.\frac{\partial u}{\partial n}\right|_s, \tag{28}$$

where v_n is the normal growth velocity, k the partition coefficient, and $\partial/\partial n$ stands for the normal derivative, the subscripts l and s indicating the liquid and solid sides of the interface. For a moving boundary, there is a need for an additional condition, which can be obtained from the balance of mass transport across the interface. As discussed above, for a molecularly rough interface the chemical potential difference across the front is small, so that transport across the front simply reduces to $\Delta\mu\equiv\mu_s-\mu_l\approx 0$. $\Delta\mu$ is a function of temperature, concentration, and stress (or strain) tensor. Any front displacement is associated with a chemical potential difference. It is shown in the appendixes that this amounts to

$$0\approx\Delta\mu=\frac{(1-\sigma^2)}{2E}(\sigma_{tt}-\sigma_{nn})^2+\gamma\tilde{\kappa}+(T_I-T_M)\frac{L}{T_M}+c_l|m_l|\frac{L}{T_M}. \tag{29}$$

The first term accounts for the increase of the solid chemical potential due to elastic deformations the second for capillary effects, the third one for the front undercooling (T_I is the actual front temperature, T_M the melting temperature of the pure solvent, and L the latent heat per unit volume), and the last one for the concentration effect (m_l is the liquidus slope). Because we consider the thermal properties of both phases to be identical, and neglect the latent heat generation at the front, T is simply given by $T=T_M+G\tilde{\zeta}$, where G is the thermal gradient. Therefore, Eq. (29) takes the form (in reduced units, i.e., $\zeta=\tilde{\zeta}/l$, $\kappa=\tilde{\kappa}l$)

$$u=1-\frac{\zeta}{l_T}-d_0\kappa-\eta\frac{(\sigma_{tt}-\sigma_{nn})^2-\sigma_0^2}{\sigma_0^2}, \tag{30}$$

where d_0 and l_T are the usual capillary and thermal lengths, reduced by the diffusion length,

$$l_T=\frac{|m_l|\Delta c}{Gl},\quad d_0=\frac{\gamma T_M}{|m_l|\Delta c L l} \tag{31}$$

while

$$\eta=\sigma_0^2\frac{(1-\sigma^2)}{2E}\frac{T_M}{|m_l|\Delta cL}. \tag{32}$$

In Eq. (30), we have subtracted from the full elastic effect the contribution corresponding to the prestrained situation. As in Sec. II, σ_0 is the applied uniaxial stress. The parameter η is associated with elasticity. It measures the ratio of the elastic energy stored due to the uniaxial stress over the latent heat of melting, which is involved to ''jump'' the temperature gap $\Delta T=|m_l|\Delta c$.

Next we have an equation relating the concentrations on the liquid and solid sides of the interface, which reads

$$u_s=k(u_l-1). \tag{33}$$

To close the description, we need equations for the elastic problem. These were already discussed and solved in Sec. II.

Note that in Eq. (30) the thermal gradient plays the same role as gravity. To see this, refer to Eq. (29) (with $T_I-T_M=G\tilde{\zeta}$), and compare with Eq. (3). One thus sees that the effective gravity is given by $g_{\rm eff}\Delta\rho\equiv GL/T_M$. For most metals $L\simeq 10$ J/$g=10^8$ erg/g and $T_m\simeq 1500$ K, and typical thermal gradients are $G\simeq 100$ K/cm, and one finds $g_{\rm eff}\simeq 10^6-10^7$ cgs$=(10^3-10^4)g$. While before we had a critical wavelength of order 1 cm given by relation (24), now, because the effective gravity $g_{\rm eff}\equiv(10^3-10^4)g$, the critical wavelength for the ATG instability can fall in the 100-μm range and hence a strong coupling with the MS instability must be expected. Because the gravity appears only with $\frac{1}{4}$th power in Eq. (24), the critical stress would be modified by about 10 only (0.1 bar instead of 0.01 bar).

IV. LINEAR STABILITY ANALYSIS

The equations of motion admit a planar front solution, the position of which differs from that of the problem without elasticity by the constant amount $h_{00}\equiv\delta\zeta=-\eta l_T$. This is due to the fact that the stress induces a solid melting (refer to Sec. III). We have absorbed this quantity into a redefinition of the z coordinate. The linear stability analysis of this solution is rather straightforward, since the elastic and diffusive problems couple only via the boundary conditions.

We start out from perturbed solutions

$$u(x,z,t)=u_0(z)+\epsilon u_1(z)\exp(iqx+\omega t), \tag{34}$$

$$\zeta(x,t)=\epsilon h(x,t)=\epsilon h_{11}\exp(iqx+\omega t), \tag{35}$$

$$\chi(x,z,t)=\chi_0(x,z)+\epsilon(a+bz)\exp(iqx+qz+\omega t), \tag{36}$$

where χ denotes the Airy function of the perturbed system, and $\chi_{\rm pre}$ that of the unperturbed prestrained system $[\chi_0(x,z)=-p(x^2/2)+(\sigma_0-p)(z^2/2)]$. The stress problem was solved in Sec. III.

Using the new boundary condition (30) in the standard linear stability analysis of the planar front in directional solidification, we arrive at the dispersion relation

$$\omega+2-2(1+q^2+\omega)^{1/2}+w_q[(1+q^2+\omega)^{1/2}+k(1+\nu^2q^2+\nu\omega)^{1/2}+k-1]=0, \tag{37}$$

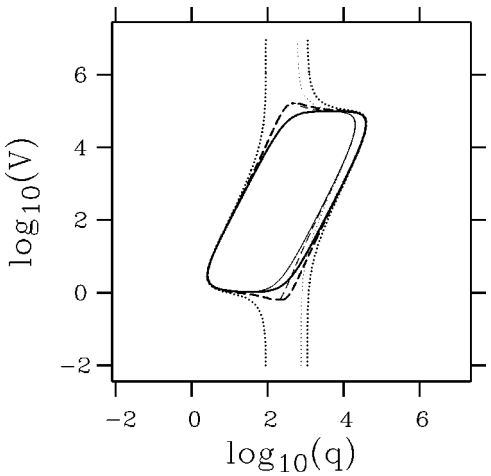

FIG. 2. The neutral curve (thick solid line) and the most dangerous mode (thin solid line) for the pure MS instability. The neutral curve in the presence of a uniaxial stress (thick dashed line), and the corresponding most dangerous mode (thin dashed line), where $\eta=0.001$ in the one-sided model. The dotted lines (neutral curve: thick dotted line; most dangerous mode: thin dotted line) correspond to $\eta=0.0015$ where no velocity threshold exists anymore $[1-4\eta^2\tilde{l}_T/\tilde{d}_0<0$; see Eq. (48)]. Here $d_0=10^{-5}$, and $k=1$, and units are chosen so that $l_T=1$ and $D=1$.

where

$$w_q=d_0q^2+\frac{1}{l_T}-4\eta q. \tag{38}$$

For $\eta=0$, we recover the Mullins-Sekerka dispersion relation. For a vanishing growth velocity (i.e., $\omega\sim l^2\gg 1$, $q\sim l\gg 1$) we can reduce the above dispersion relation in the one-sided case to

$$\omega=\sqrt{q^2+\omega}\left(4\eta q-\frac{1}{l_T}-d_0q^2\right), \tag{39}$$

which is the dynamical version of the ATG result when bulk dissipation prevails. When compared to Eq. (22), one sees that here there is an additional factor $\sqrt{q^2+\omega}$ corresponding to the situation where dissipation is supported by diffusion.

A closer analysis of Eq. (37), given in the appendixes, reveals that the principle of the exchange of stabilities holds in our system; i.e., whenever the real part of ω becomes zero, so does the imaginary part, meaning that a Hopf bifurcation does not occur from the planar state.

Figure 2 shows the neutral curve (thick solid line) and most dangerous mode (thin solid line) for $\eta=0$ and 0.001 (dashed lines). There we also show (dotted lines) the case with $\eta=0.0015$, where the surface is always unstable (see below). For typical parameter values we find that $\eta=10^{-3}$ corresponds to a uniaxial stress between 0.1 (or even smaller) and 1 bar, which is not outside the range of possible experimental situations. We can see on the figure that for a small V, the line of the most dangerous mode is concave in the presence of an uniaxial stress, and it is convex otherwise.

Given the validity of the stability exchange principle, the conditions for the instability threshold reduce to $\omega=0$ and $d\omega/dq=0$. Analytical expressions for the wave number of

the critical mode and the critical velocity may then be derived. From Eq. (37), we obtain

$$2[1-(1+q^2)^{1/2}]+w_q[(1+q^2)^{1/2}+k(1+\nu^2q^2)^{1/2}+k-1]=0, \tag{40}$$

$$w_q'[(1+q^2)^{1/2}+k(1+\nu^2q^2)^{1/2}+k-1]+q\left[\frac{w_q-2}{(1+q^2)^{1/2}}+\frac{kw_q\nu^2}{(1+\nu^2q^2)^{1/2}}\right]=0, \tag{41}$$

with

$$w_q'=2d_0q-4\eta. \tag{42}$$

Defining *effective* capillary and thermal lengths by

$$\overline{d}_0=d_0-\frac{2\eta}{q}, \tag{43}$$

$$\overline{l}_T=\frac{l_T}{1-2\eta q l_T}, \tag{44}$$

we can map the problem with elasticity to the one without. For the resulting expressions are identical to those of ordinary directional solidification [22], with d_0 replaced by $\overline{d}_0$ and l_T replaced by $\overline{l}_T$. Of course, this mapping is admissible only when the newly defined effective lengths are nonnegative.

A. Lower velocity threshold

It is then possible to take the expressions for the lower and upper thresholds of the linearly unstable range from the literature [22]. Making the appropriate substitutions, one arrives at the results for the elastic problem, providing, as we shall see, that η is small enough. Assuming $q\gg1$ and $\overline{d}_0q^2\ll1$, the low-velocity threshold is, to lowest order, given by

$$q_c=\left(\frac{k(1+\nu)}{4\overline{d}_0\overline{l}_T^2}\right)^{1/3}, \tag{45}$$

$$1=\frac{2\overline{l}_T}{1+k\nu}. \tag{46}$$

In the case of the one-sided model, the numerator of Eq. (45) must be replaced with $2k$ (but $\nu=0$ elsewhere). Note that these two equations determine q_c implicitly, since both $\overline{d}_0$ and $\overline{l}_T$ depend on q_c.

We shall characterize quantities that are given in physical units by an overtilde (if they are used both in dimensional and dimensionless form). Algebraic manipulations of the dispersion relation yield, for the critical wave number,

$$\tilde{q}_{c1}=\frac{2\eta}{\tilde{d}_0}+\frac{a\tilde{d}_0}{16\eta^2}V_{c1}^2, \tag{47}$$

a result that was obtained in Ref. [21] for the one-sided model. We have replaced the subscript c by $c1$ to emphasize the fact that this is the first of two thresholds that we consider.

The behavior described by Eq. (47) is very different from the usual proportionality $\tilde{q}_{c1}\sim V^{2/3}$ arising without the elastic term. Of course, the latter can be recovered for sufficiently small values of η, but one has to start off from Eqs (45) and (46) again, because Eq. (47) is already based on the assumption $d_0\ll\eta$.

The threshold velocity is given by

$$\frac{V_{c1}}{D}=\frac{1+k\nu}{2\tilde{l}_T}\left\{1-\frac{4\eta^2\tilde{l}_T}{\tilde{d}_0}-a\frac{\tilde{d}_0(1+k\nu)^2}{8\eta\tilde{l}_T}\left(1-\frac{4\eta^2\tilde{l}_T}{\tilde{d}_0}\right)^2\right\}, \tag{48}$$

displaying the leading terms of an expansion in powers of $1-4\eta^2\tilde{l}_T/\tilde{d}_0$. In Ref. [21], only the first term of the series was given (for the one-sided model, i.e., $\nu=0$). Evidently, in order for the critical velocity to be positive, we need $\eta^2<4\tilde{l}_T/\tilde{d}_0$. If this condition is not met, the planar interface will be unstable for arbitrarily small velocities due to the ATG instability.

It is instructive to examine the case of vanishing critical velocity. From Eqs. (47) and (48) we have $\tilde{q}_c=2\eta/\tilde{d}_0$ and $\eta^2=\tilde{d}_0/4\tilde{l}_T$, hence $\tilde{q}_c^2=1/(\tilde{d}_0\tilde{l}_T)$. Considering the pure ATG instability, we obtain

$$\tilde{q}_c=\sqrt{\frac{g_{\rm eff}\Delta\rho}{\gamma}}=\sqrt{\frac{LG}{T_M\gamma}}=\sqrt{\frac{L|m|\Delta c}{T_M\gamma}\frac{G}{|m|\Delta c}}=\sqrt{\frac{1}{\tilde{d}_0\tilde{l}_T}}, \tag{49}$$

the same result, evidently. So we may express the critical dimensionless stress for the ATG instability under the effective gravity produced by a thermal gradient and the critical wave number by the very simple formulas

$$\eta_c^{\rm ATG}=\frac{1}{2}\sqrt{\frac{d_0}{l_T}}, \tag{50}$$

$$q_c^{\rm ATG}=\sqrt{\frac{1}{d_0l_T}}. \tag{51}$$

B. Upper velocity threshold

At high velocities, the stability tongue again closes in directional solidification without elastic strain. Once more substituting effective capillary and thermal lengths to obtain the expressions with strain, we find $[g_k\equiv(1+k+k\nu^2)/2k^2]$

$$\overline{d}_0=\frac{1}{2k}-\epsilon, \tag{52}$$

$$\overline{l}_T^{-1}=\frac{\epsilon^2}{g_k}, \tag{53}$$

$$q_c^2=\frac{2\epsilon}{g_k}. \tag{54}$$

Herein, ϵ is a small parameter, measuring the distance from the absolute stability limit [22] (providing the latter exists), and hence q_c is also small.

Simple manipulations provide us with critical velocity

$$\frac{V_{c2}}{2D}=\frac{1}{\tilde{d}_0-4\eta^2\tilde{l}_T}\left[\frac{1}{2k}-\frac{1+k+k\nu^2}{8\eta^2\tilde{l}_T^2}(\tilde{d}_0-4\eta^2\tilde{l}_T)^2\right], \tag{55}$$

where the bracketed terms again constitute the beginning of a power series, this time in the variable $\tilde{d}_0-4\eta^2\tilde{l}_T$. In contradistinction with the lower velocity threshold [see Eq. (48)], the leading term of this series is independent of whether we are dealing with the one-sided model or not. It was already given in Ref. [21]. For $\eta^2=\tilde{d}_0/4\tilde{l}_T$, the upper velocity threshold diverges, i.e., the ATG instability prevents restabilization in that case.

C. Discussion of linear stability

A striking result is that despite the small value of the external stress, the neutral curve exhibits unexpected changes. For example, both the upper and lower limits of the threshold are, respectively, about ten times smaller and larger than the MS ones (note that the scales are logarithmic; Fig. 2). The dimensionless parameter η [see Eq. (32)] can be as small as 10^{-3}. As is seen from Fig. 2, even a value of $\eta\simeq 0.001$ leads to a very pronounced shift of both the minimum and maximum (close to 10). The same holds for the scale of the most dangerous modes close to the upper and lower limits (compare the thin dashed line to the thin solid line). Here elasticity favors small scales at low speed and large scales at large speed. Let us analyze Eq. (48). When $\eta^2\sim 4\tilde{l}_T/\tilde{d}_0$, no threshold exists anymore. Using the fact that $\tilde{l}_T/\tilde{d}_0\sim 10^5$, one sees that the threshold should disappear for $\eta\simeq 10^{-3}$–10^{-2}. Let us now estimate the order of magnitude for the physical uniaxial stress for which a considerable effect must be expected. For that purpose, from Eq. (32) we extract that $\sigma_0^2\simeq EL\Delta T/T_M$ ($\Delta T\equiv|m_l|\Delta c$), where the Poisson ratio (typically of order $\frac{1}{3}$) is disregarded. For many metals $L\simeq 10\,J/g=10^8$ erg/g, and $E\simeq 10^{10}$–10^{11} cgs. Finally for very dilute metals $\Delta\simeq 1$ K (and possibly smaller), while the melting temperature lies in the range 1000–1800 K. This amounts on the average to $\sigma_0\simeq 10^6$ cgs, or equivalently a stress corresponding to the atmospheric pressure. For more dilute and soft materials with ''weak'' crystallization (small ΔT, E, and L), it seem feasible to reach critical values of $\sigma_0\simeq 0.1$–0.01 bar. Thus it appears that the effect we have put forward can be checked experimentally by applying moderate pressures. The same effect is expected on the wave numbers; variations of one decade by application of a uniaxial stress of the order of a fraction of the atmospheric pressure.

If the tongue is preserved (i.e., $\eta^2<4\tilde{d}_0/\tilde{l}_T$), and for typical values given in the caption of Fig. 2, we find that $V_{c1}/V_{\mathrm{ms}1}\sim 7$, $q_{c1}/q_{\mathrm{cms}1}\sim 4$, while $V_{c2}/V_{\mathrm{ms}2}\sim 40$ and $q_{c2}/q_{\mathrm{cms}2}\sim 20$, where the subscript ms refers to the bare Mullins-Sekerka value. The fact that elastic effect is much more pronounced in the large velocity regime is understood as follows. At large velocity the diffusion length becomes smaller and smaller. The self-interaction of the front becomes local, and usually capillary effects overcome the diffusive instability. Since elasticity always acts on large scales, it wins over diffusion and determines the dynamics at large scales (q small).

V. WEAKLY NONLINEAR BEHAVIOR

The main outcome of the linear theory is the determination of the condition for the onset of the instability and the range of modes which are likely to grow first. In order to obtain information beyond the instability threshold, a nonlinear analysis is necessary. In a first step, we restrict ourselves to an analysis of the weakly nonlinear behavior to determine the nature of the bifurcation. This analysis, which is standard [23,11], consists of an expansion in powers of the amplitude of the deformation up to third order.

If $A(t)$ is the instantaneous deformation amplitude, the resulting equation will take the form

$$\frac{dA}{dt}=\omega A+a_1A^3. \tag{56}$$

We recall that ω is the linear growth rate determined in Sec. IV, whereas a_1 is the Landau constant, the sign of which tells us whether the bifurcation is subcritical ($a_1>0$) or supercritical ($a_1<0$).

So our goal will be to determine this constant. This approach has been applied to directional solidification before [11], so we can be brief in our description of the procedure, and will just give the basic equations and results. For ease of presentation, we will consider the one-sided model only.

We look for solutions to the equations of motion (27) and (7), given the pertinent boundary conditions (28) and (30), in the forms

$$u(x,z,t)=\sum_{n=0}^{\infty}\epsilon^n u_n(x,z,t), \tag{57}$$

$$\chi(x,z,t)=\sum_{n=0}^{\infty}\epsilon^n \chi_n(x,z,t), \tag{58}$$

$$\zeta(x,t)=\epsilon h(x,t)=\sum_{n=0}^{\infty}\epsilon^n h_n(x,t), \tag{59}$$

and assume that

$$u_1(x,z,t)=A(t)\cos(qx)u_1(z), \tag{60}$$

$$\chi_1(x,z,t)=A(t)\cos(qx)\chi_1(z), \tag{61}$$

$$h_1(x,t)=A(t)\cos(qx), \tag{62}$$

where $u_1(z)$ and $\chi_1(z)$ constitute the solution to the linearized problem. Inserting Eqs. (57)–(62) into the basic equations, one arrives in a straightforward manner at

$$u_2(x,z,t)=A^2(t)[u_{20}(z)+u_{22}(z)\cos(2qx)], \tag{63}$$

$$u_3(x,z,t)=A^3(t)[u_{31}(z)\cos(qx)+u_{33}(z)\cos(3qx)], \tag{64}$$

as well as

$$h_2(x,t)=A^2(t)[h_{20}+h_{22}\cos(2qx)], \tag{65}$$

$$h_3(x,t)=A^3(t)[h_{31}\cos(qx)+h_{33}\cos(3qx)], \tag{66}$$

and similar expressions for $\chi(x,z,t)$, which we do not write out here. Truncating the expansion at order 3, we obtain Eq. (56) for the temporal evolution of the amplitude $A(t)$ with $a_1/\omega=O(\epsilon^2)$. To obtain the third-order result for the full problem, we will need to evaluate χ only up to second order [12]; its form is then

$$\chi(x,z)=\sigma_0[(s_{11}z+s_{10})\cos(qx)e^{qz} + (s_{21}z+s_{20})\cos(2qx)e^{2qz}]. \tag{67}$$

The solutions to the second-order problem yield

$$u_{20}(z)=u_{20}e^{-\mu_{20}z}, \quad u_{22}(z)=u_{22}e^{-\mu_{22}z}, \tag{68}$$

where $\mu_{20}=1+\sqrt{1+2\omega}$ and $\mu_{22}=1+\sqrt{1+2\omega+4q^2}$. Solving the elastic problem, thus obtaining the coefficients s_{20} and s_{22}, from the surface equations we obtain two linear systems of equations determining the pairs (h_{20},u_{20}) and (h_{22},u_{22}), respectively. The coefficients are collected in the appendixes (for the limit $\omega=0$).

For a calculation of the Landau coefficient a_1, it is sufficient to compute the terms involved in the equation for u_{31}. The bulk equations contain a contribution due to the third-order term proportional to $\cos(qx)$ that appears in the time derivative of u_1. Therefore, the equation for $u_{31}(z)$ takes the the form

$$\frac{\partial^2 u_{31}}{\partial z^2}+2\frac{\partial u_{31}}{\partial z}=\omega u_{31}+a_1(2-w_q)e^{-\mu_l z}, \tag{69}$$

where $\mu_l=1+\sqrt{1+q^2+\omega}$, and w_q has been given in Eq. (38). The pertinent solution to Eq. (69) reads

$$u_{31}(z)=u_{31}e^{-\mu_{31}z}+\frac{a_1(2-w_q)}{2\omega}(e^{-\mu_{31}z}-e^{-\mu_l z}), \tag{70}$$

where $\mu_{31}=1+\sqrt{1+3\omega+q^2}$. In the limit $\omega\to 0$, the two exponents are equal, and the solution becomes

$$u_{31}(z)=\left(u_{31}-\frac{a_1(2-w_q)}{\sqrt{1+q^2}}z\right)e^{-\mu_l z}. \tag{71}$$

From the boundary conditions for the diffusion field [Eqs. (30) and (28)], we find two inhomogeneous linear equations relating h_{31} and u_{31}:

$$L\begin{pmatrix}h_{31}\\u_{31}\end{pmatrix}=\mathbf{F}(q,l_T,\eta,k). \tag{72}$$

The linear operator L on the left-hand side is a matrix the determinant of which vanishes at the bifurcation. This means that the vector $\mathbf{F}$ on the right-hand side must satisfy a solvability condition: it must be orthogonal to the left-side eigenvector of L corresponding to the eigenvalue zero. (More down to earth: the two components F_1 and F_2 must have a given ratio.) This solvability condition fixes the value of a_1 in terms of the system parameters.

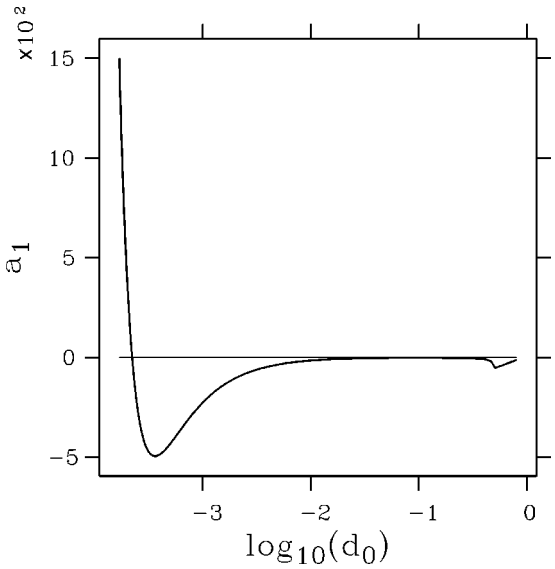

FIG. 3. The Landau constant as a function of the reduced capillary length. A negative a_1 corresponds to a supercritical bifurcation. $\eta=1.5\times10^{-3}$.

The result is

$$a_1=u_{22}\left[\frac{\mu_{22}}{2}(\mu_l-\mu_{22})+q^2\right]+u_{20}[\mu_{20}(\mu_l-\mu_{20})] + h_{22}[(2-w_q)q^2-2\mu_l+4] - [\mu_l+2(k-1)]x_q-\frac{2-w_q}{4}\mu_l q^2+\mu_l-2. \tag{73}$$

The pure ATG instability is known to be subcritical [12]. We have checked that our result reduces to that of Nozières [12] in the limit $V\to 0$. The Mullins-Sekerka instability may be subcritical or supercritical depending on the velocity and the partition coefficient. For small velocities the MS bifurcation is subcritical [11] for $k<0.45$ (which is the case for the majority of metals) and supercritical otherwise. Here we find that in the small V or equivalently large q regime the (third-order) Landau constant is dominated by the ATG effect which behaves as q^4; the MS effect behaves as q^2. However as V increases (or, equivalently, on increasing d_0, the reduced capillary length—recall that it is reduced by the diffusion length), and if the MS bifurcation is supercritical (ensured by not too small a partition coefficient), one finds a transition from a subcritical bifurcation into a supercritical one. The result is shown in Fig. 3. Since the critical velocity for the change of regime is not too large, this result is not devoid of experimental testability.

VI. SUMMARY OF IMPORTANT RESULTS AND CONCLUSIONS

Let us first summarize the main results of this paper.

(i) We have shown that the MS and the ATG instabilities are strongly coupled. The main reason for this is that they

both operate in directional solidification at similar length scales (about 100 μm). The effect should be visible experimentally upon an application of a stress (most likely by means of piezoelectric plates) of order 0.1–1 bar. The critical physical velocity of the usual MS instability is given, for the one sided model, by [approximately; see Eq. (48)]

$$\frac{V_{c1}}{D}=\frac{1}{2\tilde{l}_T}\left\{1-\frac{4\eta^2\tilde{l}_T}{\tilde{d}_0}\right\}, \tag{74}$$

where we recall that $\tilde{l}_T$ is the thermal length, $\tilde{d}_0$ the capillary length, and η is related to the applied stress and is given by Eq. (32). The critical velocity is lowered by the applied stress. In the extreme limit where $\eta^2=4\tilde{l}_T/\tilde{d}_0$, the critical velocity vanishes. This equality requires a stress of order 0.1–1 bar. By approaching this value, we expect the instability to develop at arbitrary small growth velocities.

(ii) The stress has an important effect on the critical wavelength. We have found that typically the critical wave number behaves as

$$\tilde{q}_{c1}=\frac{2\eta}{\tilde{d}_0}+\frac{2k\tilde{d}_0}{16\eta^2}V_{c1}^2. \tag{75}$$

On the one hand, the dependence on velocity is completely different from that of pure MS bifurcation (which leads to a dependence like $V^{2/3}$, to be compared to an exponent which is three times larger). This effect is clearly not devoid of experimental testability. On the other hand, the value of the wave number is found (for the parameters used in the caption of Fig. 2) to be about four times larger than that of the pure MS one (larger values are possible by increasing the stress). Thus application of a stress should lead to a finer structure.

(iii) At large enough velocities, elastic effects are even more pronounced. If q_c is small enough (the physical wave number is small in comparison to the inverse of the diffusion length), then Eq. (55) gives, as a threshold value (after transforming the variables back into physical dimensions),

$$V_{c2}=\frac{D}{k(\tilde{d}_0-4\eta^2\tilde{l}_T)}, \tag{76}$$

where the subscript 2 is a reminder that we consider the upper velocity threshold. In the absence of stress, $V_{c2}=D/k\tilde{d}_0$, expressing that the diffusion length is twice the capillary length. In the presence of stress, the velocity restabilization is increased. Using the values used in the caption of Fig. 2, we find that V_{c2} is about seven times that of the pure MS case.

The critical wave number also varies with stress. Its expression is obtained from Eq. (54) by using the above relation for the bifurcation [which can be rewritten to leading order as $\eta^2 l_T=(d_0-1/2k)/4$]

$$q_c\simeq(8/3)\,\eta/\epsilon, \tag{77}$$

where we have set $1+\sqrt{1-8/9}\simeq 1$, and ϵ is the distance from the absolute stability limit. Typically for an ordinary gradient, $\epsilon\simeq 0.1$–0.01. Let us compare the present q_c to that obtained in the pure MS case. In that case $q_{c\mathrm{MS}}^2=[4k^2/(1+k)]\epsilon$. Thus the ratio takes the form

$$\frac{q_c}{q_{c\mathrm{MS}}}\simeq\frac{8\eta\sqrt{1+k}}{6k\epsilon^{3/2}}. \tag{78}$$

For parameters given in the caption of Fig. 2, we find that $q_c/q_{c\mathrm{MS}}\sim 1/20$ (where we have chosen $\epsilon=0.1$ and $k\simeq 1$). For a smaller partition coefficient (the case of many metallic alloys) the effect is even more pronounced. That is to say the wavelength is increased at large velocities by a large amount.

(iv) We have studied the nonlinear evolution of the bifurcation by deriving a Landau constant whose sign determines the nature of the bifurcation. The pure ATG instability is subcritical according to Nozières's calculation [12]. At the lower velocity threshold, the MS bifurcation is subcritical if k is small ($k<0.44..$) and supercritical otherwise. We have shown here that if k is large enough, the bifurcation becomes supercritical due to the MS bifurcation nature. If k is small enough, then the ATG-MS bifurcation will remain subcritical.

It is worthwhile to note that the present work could be of some relevance in the context of the formation of giants causeway in igneous rocks. These are patterns that are known in the geology literature [24] to form by contraction during cooling and crystallization of the lava. We hope to report on quantitative results in the near future.

Finally an important task concerns the experimental testability of our finding. A possibility would be to use a cell with piezoelectric plates in order to impose a controlled uniaxial stress on the solid, as was devised for ^{4}He by Balibar and co-workers [7].

Transparent materials such as succinonitrile are not, in our opinion, suitable, since these have plastic properties. This does not mean so far that plastic behaviors may not lead to interesting features. But this question is beyond the present study. Of course transparent materials have interesting properties, such as the allowance for an *in situ* analysis, and it would be very important to take advantage of that. However, many materials that enter this category not only possess plasticity, but are smooth on the atomic scale, and therefore exhibit faceted morphologies. In contrast many metallic alloys are rough on the atomic scale, and lead to rounded growth shapes. We believe that metallic alloys are important candidates on which to perform such experiments. By now there exists an overabundant literature about directional solidification on these materials. The effects we put forward should be easily detectable since they involve strong changes both on the threshold values and the scales of the pattern. We believe that experimental checks of our theory are decisive in order to guide further developments.

ACKNOWLEDGMENTS

This work was supported by a ''PROCOPE'' grant in the framework of a French-German cooperation.

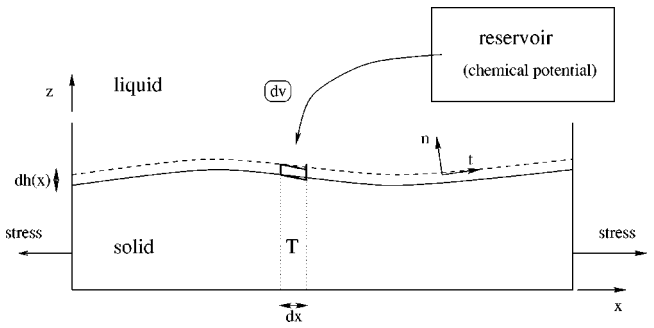

FIG. 4. Calculation of the surface potential.

APPENDIX A: DERIVATION OF CHEMICAL POTENTIALS

1. Pure ATG instability

In order to obtain the difference in chemical potential between the liquid and solid phases, we consider a reference state, in which the two phases are at equilibrium, and calculate the change in the Gibbs free energy of the system on transforming a small mass element of liquid at the interface into solid (see Fig. 4). We denote the volume of the transformed solid by δV.

The total change of the Gibbs free energy will then be

$$\Delta G=\Delta F+\Delta(p_l V)\equiv \delta V\Delta\mu(x,\zeta(x)), \tag{A1}$$

as we are referring the chemical potential not to mass but to the equivalent solid volume. Here ΔF is the change in Helmholtz free energy. This quantity can be decomposed into three parts,

$$\Delta F=\Delta F_b+\Delta F_i+\Delta F_v\,, \tag{A2}$$

where ΔF_b corresponds to the change in free energy of the bulk phases, ΔF_i is the interface part, and ΔF_v is the free energy change of the transformed mass element. The first contribution ΔF_b is zero, because the bulk phases are not modified, except at the position of phase transformation, the contribution of which is explicitly taken into account in the last term. The second contribution, the change in surface free energy, arises from surface tension $\Delta F_i=\gamma\delta A$, with δA the change in surface area, whereas the last contribution has to be calculated from the work necessary to bring a volume element of solid to the appropriate position in the gravitational field, and to increase its internal strain to the prevailing value. This is obtained by integrating the work for an infinitesimal change [14]

$$df=\sigma_{ij}du_{ij}+\rho g\,d\zeta. \tag{A3}$$

Therefore, this latter contribution is naturally split up into an elastic and a gravitational piece.

For the differential of the elastic contribution to ΔG, we may thus write

$$\begin{aligned} dG_{\rm el}&=\sigma_{ij}du_{ij}\delta V+p_l d(\delta V)\\ &=[(\sigma_{nn}du_{nn}+\sigma_{tt}du_{tt})-\sigma_{nn}(du_{nn}+du_{tt})]\delta V\\ &=(\sigma_{tt}-\sigma_{nn})du_{tt}\delta V, \end{aligned} \tag{A4}$$

where we have used the condition of mechanical equilibrium at the boundary in a twofold way: first, the condition $\sigma_{nt}=0$ tells us that the stress tensor is diagonal in the coordinate system spanned by the normal and tangential vectors **n** and **t**; second, we have replaced the liquid pressure p_l with $-\sigma_{nn}$, neglecting the cross-term between elasticity and capillarity. Moreover, we have expressed the local change of the volume element δV in terms of the appropriate strain expressions $d\,\delta V=\mathrm{Tr}(du_{ij})\,\delta V$.

Our next approximation is to neglect the cross-term between gravity and elasticity, arising from the change in pressure due to the height change produced by the volume element. Therefore, we can assume that σ_{nn} is constant. Then we obtain, from Hooke's law [Eq. (1)],

$$du_{tt}=\frac{1-\sigma^2}{E}d\sigma_{tt}=\frac{1-\sigma^2}{E}d(\sigma_{tt}-\sigma_{nn}). \tag{A5}$$

Inserting this into Eq. (A4), and integrating to finite stress differences, we arrive at

$$\Delta G_{\rm el}=\frac{1-\sigma^2}{2E}(\sigma_{tt}-\sigma_{nn})^2\delta V. \tag{A6}$$

In a way, the calculation of the gravity part is the most subtle piece of the evaluation of ΔG. Since in order to obtain a volume δV of the solid, we have to solidify a *different* volume $(\delta V\rho_l/\rho_s)$ of the liquid, it looks, at first sight, as if the equilibrium condition at the interface becomes nonlocal, because we need to fill in the missing liquid volume (providing $\rho_s>\rho_l$) with liquid from elsewhere, and we should have to specify from where it came. For example, if we know the initial height of the liquid level above the solid, it is easy to see that the change in potential energy in the gravitational field on solidifying a small piece of liquid will depend on that height. However, we will take the point of view here that this dependence is absorbed into the equilibrium height of the interface. We formulate our discussion in terms of free energy rather than potential energy. It is then found that we have to take into account two terms; one is the integral of the second term in Eq. (A3), the other arises from the variation of the hydrostatic pressure with height: $dp_l=-\rho_l g\,d\zeta$. The total contribution then becomes

$$\Delta G_{\rm grav}=\Delta\rho g\,\zeta(x)\,\delta V. \tag{A7}$$

For the surface energy contribution, we simply have to note that in the case of one-dimensional deformations the surface change is proportional to the change of arc length in the plane of the deformations. Because the curvature is the variational derivative of ds/dx, where $s=\int^x\sqrt{1+\zeta'(x)^2}dx$ is the arc length,

$$\kappa=\frac{\delta\ ds/dx}{\delta\zeta(x)}, \tag{A8}$$

we have

$$\delta A=\int\frac{\delta s'(x)}{\delta\zeta(x)}dx\,d\zeta\ \ dy=\kappa\delta V, \tag{A9}$$

and hence

$$\Delta G_{\mathrm{cap}} = \gamma \kappa \delta V. \tag{A10}$$

Collecting the terms from Eqs. (A6), (A7), and (A10), and dividing by δV, we obtain

$$\Delta \mu = \frac{1-\sigma^2}{2E}(\sigma_{tt}-\sigma_{nn})^2 + \gamma\tilde{\kappa} + \Delta\rho g \tilde{\zeta}(x), \tag{A11}$$

which is identical to Eq. (3).

2. Directional solidification

Here we will derive the chemical potential difference between the solid and liquid phases in directional solidification without regard to elastic effects. Then, in the same spirit as before, neglecting cross terms, we will add the elastic contribution.

The condition for chemical equilibrium of the solute is

$$c_s = k c_l. \tag{A12}$$

To obtain the interface temperature, giving us its position via $T = T_0 + G\zeta$, we will write down the chemical potential of the solvent; exploiting that we have a dilute alloy, we do this calculation by an expansion about the point of reference describing the pure substance

$$c_{l0} = c_{s0} = 0, \quad T = T_M, \quad p_{l0} = p_{s0} = p_l(T_M). \tag{A13}$$

This point of reference corresponds to an equilibrium situation, hence we have $\mu_{l0} = \mu_{s0}$. Thus we obtain $\Delta\mu = \mu_s - \mu_l$ directly:

$$\Delta\mu = c_s \frac{\partial \mu_s}{\partial c} + \gamma\tilde{\kappa}\frac{\partial \mu_s}{\partial p} + (T_I - T_M)\frac{\partial \mu_s}{\partial T} - c_l \frac{\partial \mu_l}{\partial c} - (T_I - T_M)\frac{\partial \mu_l}{\partial T}. \tag{A14}$$

The partial derivatives of μ with respect to pressure and with respect to temperature are known (recall that we refer the chemical potential to the unit volume):

$$\left.\frac{\partial \mu}{\partial p}\right|_{T,c} = 1, \quad \left.\frac{\partial \mu}{\partial T}\right|_{p,c} = -s, \tag{A15}$$

where s is the entropy density (entropy per volume). Evidently, the latent heat per volume can be expressed via the entropy density

$$L = T_M(s_l - s_s). \tag{A16}$$

The combination of partial derivatives with respect to concentration that appears in Eq. (A14) is obtainable from the phase diagram (see Fig. 5). Phase equilibrium along the liquidus and solidus lines is expressible as

$$\frac{\partial \mu_s}{\partial T} + \frac{dc_s}{dT}\frac{\partial \mu_s}{\partial c} = \frac{\partial \mu_l}{\partial T} + \frac{dc_l}{dT}\frac{\partial \mu_l}{\partial c} \tag{A17}$$

$$\Leftrightarrow \quad k\frac{\partial \mu_s}{\partial c} - \frac{\partial \mu_l}{\partial c} = |m_l|(s_s - s_l) = |m_l|\frac{L}{T_M}.$$

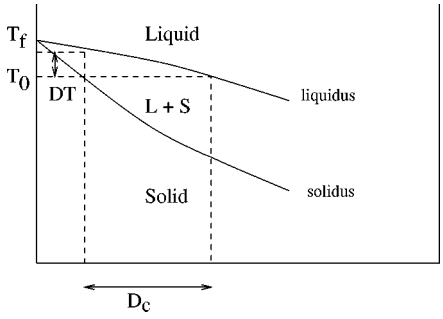

FIG. 5. Phase diagram of a dilute alloy.

Finally, collecting the terms, we find

$$\Delta\mu = \gamma\tilde{\kappa} + (T_I - T_M)\frac{L}{T_M} + c_l|m_l|\frac{L}{T_M}. \tag{A18}$$

Adding in the stress expression, we arrive at Eq. (29).

On replacing T_I in this equation by $T_0 + G\tilde{\zeta}$, we note the analogy of the term $GL\tilde{\zeta}/T_M$ with the term $\Delta\rho g\tilde{\zeta}$ in Eq. (A11). This means we can describe this expression as equivalent, for the ATG instability, to an effective gravity of magnitude $g_{\mathrm{eff}}\Delta\rho = GL/T_M$. A calculation with typical values for the thermal quantities shows that $g_{\mathrm{eff}}\Delta\rho$ exceeds $g\Delta\rho$ by at least four orders of magnitude (see Sec. III). Therefore, we are entitled, in combining Eqs. (A11) and (A18), to neglect the true gravity term in comparison with the effective one.

APPENDIX B: STABILITY EXCHANGE PRINCIPLE

Setting $\omega = \omega_r + i\omega_i$ in Eq. (37), we obtain the neutral surface separating stable and unstable regions of parameter space by requiring the real part ω_r to vanish. This leads to the following set of two real equations:

$$2 - \sqrt{2}x_1 + w_q\left(\frac{x_1}{\sqrt{2}} + k\frac{x_2}{\sqrt{2}} + k - 1\right) = 0, \tag{B1}$$

$$|\omega_i|\left[1 - \frac{\sqrt{2}}{x_1} + w_q\left(\frac{1}{\sqrt{2}x_1} + \frac{k\nu}{\sqrt{2}x_2}\right)\right] = 0. \tag{B2}$$

Herein, we have introduced the abbreviations

$$x_1 = \{[(1+q^2)^2 + \omega_i^2]^{1/2} + 1 + q^2\}^{1/2}, \tag{B3}$$

$$x_2 = \{[(1+\nu^2 q^2)^2 + \nu^2\omega_i^2]^{1/2} + 1 + \nu^2 q^2\}^{1/2}, \tag{B4}$$

which are related to the square root expressions in Eq. (37) [for $\omega_r = 0$] via

$$(1 + q^2 + i\omega_i)^{1/2} = \frac{1}{\sqrt{2}}\left(x_1 + i\frac{\omega_i}{x_1}\right), \tag{B5}$$

$$(1 + \nu^2 q^2 + i\nu\omega_i)^{1/2} = \frac{1}{\sqrt{2}}\left(x_2 + i\nu\frac{\omega_i}{x_2}\right). \tag{B6}$$

Note that we have defined square roots to have a positive real part.

Let us now *assume* that there are solutions to the system of equations (B1) and (B2), with $\omega_i \neq 0$, i.e., that the stability exchange principle *does not hold*. Then Eq. (B2) implies the vanishing of the bracket term, so we obtain

$$w_q\left(\frac{x_1}{\sqrt{2}}+k\frac{x_2}{\sqrt{2}}+k-1\right)=\sqrt{2}x_1-2, \tag{B7}$$

$$w_q\left(\frac{1}{\sqrt{2}x_1}+\frac{k\nu}{\sqrt{2}x_2}\right)=\frac{\sqrt{2}}{x_1}-1. \tag{B8}$$

From its definition, we see that $x_1>\sqrt{2}$, and thus the parentheses on the left-hand sides of Eqs. (B7) and (B8) are positive, while the right-hand side of Eq. (B7) is positive and that of Eq. (B8) is negative. Thus we find $w_q>0$ from Eq. (B7) and $w_q<0$ from Eq. (B8), which is a contradiction. Therefore, our assumption $\omega_i \neq 0$ was wrong, and the principle of stability exchange must hold. For $\omega_i=0$, Eq. (B2) is satisfied automatically, and Eq. (B8) is not implied. The conclusion from Eq. (B7) remains correct: $w_q>0$ on the neutral surface. Hence we have demonstrated that the bifurcation from the planar interface never is of the Hopf type.

APPENDIX C: AMPLITUDES IN WEAKLY NONLINEAR ANALYSIS

First, we give the coefficients appearing in the expression for χ to second order:

$$\begin{aligned}
s_{10}&=(\alpha A)^3\left(-\frac{3q}{4}+\frac{h_{22}}{2}\right),\\
s_{11}&=-\alpha A+(\alpha A)^3\left(\frac{3q^2}{8}+\frac{5qh_{22}}{2}\right),\\
s_{20}&=\frac{1}{4}(\alpha A)^2,\\
s_{21}&=(\alpha A)^2\left(\frac{q}{2}-h_{22}\right).
\end{aligned} \tag{C1}$$

Then the elasticity term in Eq. (30), $s\equiv(\sigma_{tt}-\sigma_{nn})^2-\sigma_0^2/\sigma_0^2$, becomes

$$\begin{aligned}
s=&S_1\alpha A\cos(qx)+[S_{20}+S_{22}\cos(2qx)](\alpha A)^2\\
&+[S_{31}\cos(qx)+S_{33}\cos(3qx)](\alpha A)^3,
\end{aligned} \tag{C2}$$

with

$$\begin{aligned}
S_1&=-4q,\\
S_{20}&=0,\\
S_{22}&=4q^2-8h_{22}q,\\
S_{31}&=6q^3+8q^2h_{22}-4qh_{13}.
\end{aligned} \tag{C3}$$

The coefficients appearing in the calculation of the concentration field and of the interface position are

$$\begin{aligned}
u_{20}&=-1+\tfrac{1}{2}(2-w_q)\mu_l,\\
h_{20}&=0,\\
u_{22}&=H^{-1}\{4k[-1+\mu_l\tfrac{1}{2}(2-w_q)-4\eta q^2]\\
&\quad+(2-w_{2q})[2k-(2-w_q)(q^2+k\mu_l)]\},\\
h_{22}&=H^{-1}\{2k-(2-w_q)(q^2+k\mu_l)\\
&\quad-[\mu_{22}+2(k-1)][1+4\eta q^2-\mu_l\tfrac{1}{2}(2-w_q)]\},
\end{aligned} \tag{C4}$$

where we have used the notations

$$\begin{aligned}
H&=4k-(2-w_{2q})[\mu_{22}+2(k-1)],\\
w_q&=l_T^{-1}-4\eta q+d_0q^2,\\
w_{2q}&=l_T^{-1}-8\eta q+4d_0q^2,\\
x_q&=\eta(6q^3+8q^2h_{22})-\frac{3d_0q^4}{8}.
\end{aligned} \tag{C5}$$

In the limit $\eta=0$, these results become identical to those of Wollkind and Segel [23].

[1] W. W. Mullins and R. F. Sekerka, J. Appl. Phys. **35**, 444 (1964).
[2] H. Esaka and W. Kurz, J. Cryst. Growth **72**, 578 (1985).
[3] S. de Cheveigné and C. Guthmann, J. Phys. I **2**, 193 (1992); J. T. C. Lee and R. A. Brown, Phys. Rev. B **47**, 4937 (1993).
[4] K. Kassner, C. Misbah, H. Müller-Krumbhaar, and A. Valance, Phys. Rev. E **49**, 5477 (1994); **49**, 5495 (1994).
[5] M. A. Grinfeld, Dokl. Akad. Nauk. SSSR **290**, 1358 (1986) [Sov. Phys. Dokl. **31**, 831 (1986)].
[6] R. J. Asaro and W. A. Tiller, Metall. Trans. A **3**, 1789 (1972).
[7] S. Balibar, D. O. Edwards, and W. F. Saam, J. Low Temp. Phys. **82**, 119 (1991); R. H. Torri, and S. Balibar, *ibid.* **89**, 391 (1992).
[8] K. Kassner and C. Misbah, Europhys. Lett. **28**, 245 (1994).
[9] R. Nötzel, J. Temmyo, and T. Tamamura, Nature (London) **369**, 131 (1994).
[10] S. R. Tait and C. Jaupart, *Interactive Dynamics of Convection and Solidification, NATO Advanced Study Institute,* edited by H. Davis, H. E. Huppert, U. Müller, and M. G. Worster (Kluwer, Dordrecht, 1992).
[11] B. Caroli, C. Caroli, and B. Roulet, J. Phys. (France) **43**, 1767 (1982).
[12] P. Nozières, J. Phys. I **3**, 681 (1993).
[13] P. Nozières, (unpublished).
[14] See L. D. Landau and E. Lifchitz, *Theory of Elasticity* (Mir, Moscow, 1967).
[15] C. Misbah (unpublished).
[16] B. J. Spencer, P. W. Voorhees, S. H. Davis, and G. B. McFadden, Acta Metall. Mater. **40**, 1599 (1992).
[17] I. N. Stranski and Von L. Krastanow, Akad. Wiss. Lit. Mainz Abh. Math. Naturwiss. Kl. IIb **146**, 797 (1939).

[18] D. Eaglesham and M. Cerrulo, Phys. Rev. Lett. **64**, 1943 (1990).
[19] R. Nötzel, J. Temmyo, and T. Tamamura, Nature (London) **369**, 131 (1994).
[20] C. Misbah (unpublished).
[21] I. Durand, K. Kassner, C. Misbah, and H. Müller-Krumbhaar, Phys. Rev. Lett. **76**, 3013 (1996).
[22] K. Kassner, *Pattern Formation in Diffusion-Limited Crystal Growth* (World Scientific, Singapore, 1996).
[23] D. J. Wollkind and L. A. Segel, Trans. R. Soc. S. Afr. **268**, 351 (1970).
[24] See, for example, S. Chernicoff, *Geology* (Worth, New York, 1995).